COMMUNICATIONS CHEMISTRY

ARTICLE

DOI: 10.1038/s42004-018-0035-x OPEN

Symmetry-based rational design for boosting chiroptical responses

Hiroki Tanaka[1], Mina Ikenosako[1], Yuka Kato[2], Michiya Fujiki[2], Yoshihisa Inoue[1] & Tadashi Mori[1]

Chiral molecules play indispensable roles in advanced materials and technologies. Nevertheless, no conventional, yet reliable logical strategies are available for designing chiral molecules of desired chiroptical properties. Here, we propose a general protocol for rationally aligning multiple chiral units to boost the chiroptical responses, using hexahelicene as a prototype. In this proof-of-concept study, we align two hexahelicenes in various orientations and examine by theoretical calculations to predict the best chiroptical performance for X-shaped and S-shaped double hexahelicenes. We synthesize and optically resolve both double hexahelicenes and show that they exhibit more than a twofold increase in intensity of circular dichroism and circularly polarized luminescence, experimentally validating the protocol. The enhanced chiroptical responses are theoretically assignable to the electric and magnetic transition dipole moments of component hexahelicenes aligned in the correct symmetry. A guiding principle for designing advanced molecular and supramolecular chiral materials is further discussed.

[1] Department of Applied Chemistry, Graduate School of Engineering, Osaka University, 2-1 Yamada-oka, Suita, Osaka 565-0871, Japan. [2] Graduate School of Materials Science, Nara Institute of Science and Technology, Ikoma, Nara 630-0101, Japan. Correspondence and requests for materials should be addressed to T.M. (email: tmori@chem.eng.osaka-u.ac.jp)

Possessing unique chiroptical properties, chiral organic molecules[1,2] are indispensable components of next-generation smart materials used in various disciplines. Theoretically, all chiroptical properties are related to rotational strength (R), which is defined as the imaginary part of scalar product of the relevant electric ($\boldsymbol{\mu}_e$) and magnetic ($\boldsymbol{\mu}_m$) transition dipole moments:[3–5]

$$R = \mathrm{Im}(\boldsymbol{\mu}_e \cdot \boldsymbol{\mu}_m) = |\boldsymbol{\mu}_e||\boldsymbol{\mu}_m| \cos\theta \quad (1)$$

The degree of dissymmetry is quantified by the dissymmetry factor ($g = 4R/D$), which incorporates the transition probability (dipole strength D). However, the factors and mechanism that control the chiroptical responses in real molecules are not well understood and practically no reliable guidelines have been established for rationally designing chiral molecules with desired chiroptical responses[6]. Thus, the occasional successes in improving chiroptical properties of organic molecules have been achieved mostly on a trial-and-error basis through inspiration or by chance[7–9].

Here we show a general protocol for rationally aligning multiple chiral units to boost the chiroptical responses, using hexahelicene as a prototype. In this proof-of-concept study, we demonstrate that aligning two hexahelicenes (**HH**s) in X-shaped and S-shaped forms can induce more than twice intensified circular dichroism (CD) and circularly polarized luminescence (CPL). Our combined experimental and theoretical investigations also reveal how the molecular symmetry and the alignment of chiral elements determine the CD and CPL responses by manipulating electric and magnetic transition dipole moments of the molecule. The current study provides a reliable guiding principle for designing novel advanced chiral molecules and materials with strong chiroptical responses.

Results

Search for better arrangement of chiral units. Helicenes[10–13] are inherently chiral *ortho*-fused aromatics and their ground- and excited-state chiroptical properties have been utilized in various fields, including chirality sensing, chiral chromatography, chiral optical force, on-surface asymmetric synthesis, spin filter and CPL materials[14–18]. In this study, we employed **HH**[19,20] as a prototypical chiral unit to explore the rational protocol for improving the circular dichroism and CPL responses by properly aligning in space (and eventually merging) multiple **HH** molecules.

Figure 1 illustrates the examined alignments of two (*P*)-screw chiral **HH** units placed horizontally (**W**, **S**, $\mathbf{C_2}$, and **X**) or stacked vertically (**Z**) at the van der Waals (vdW) contact distance, all of which were subjected to the computational study for assessing how and to what extent the chiroptical responses are affected by the alignment. We chose the cost-effective time-dependent density functional theory (TD-DFT) with M06-2X functional for estimating the absorption dissymmetry factor (g_{abs}) for the main (^1B_b) band relative to that of **HH** (Supplementary Table 3). As can be seen from the bar graph in Fig. 1, the D_2-symmetrically or C_2-symmetricallly assembled **S**, **X**, and **Z** outperform the simply sled **W** and $\mathbf{C_2}$, affording much enhanced relative g_{abs} factors of 2.3–4.4 (against **HH**) for the former but comparable or even worse 0.7–1.1 for the latter. However, repeating twice the **S**, **X**, or **Z** assembly in the same direction (**SS**, **XX**, and **ZZ**) is not or less effective in further improving the already enhanced g_{abs} factors; see the values in the parentheses in Fig. 1.

Of particular interest, the g factor turned out to be less sensitive to the inter-helicene distance. For instance, the relative g factor of **S** at the vdW distance (4.4) was practically kept unchanged (4.4–4.8) upon separation by 1–10Å, due probably to the effective coupling of electric and magnetic transition moments of each chromophore (vide infra). The g factors calculated for **X** behaved similarly, varying from 2.3 to 1.5 upon separation of two component **HH**s by 1 to 10 Å. This means that the component chiral units should not necessarily be in the vdW contact but can be separated and placed in supramolecular, macromolecular and crystal lattices and channels, leaving us much freedom in designing chiroptical materials of higher performance.

Because of the greater enhancement upon double and/or quadruple assembling (Fig. 1), we chose the **S** and **X** assemblies for the experimental verification of the theoretical predictions. Since precisely aligning two **HH** units in a desired geometry is not a trivial task and the inter-chromophore distance does not greatly affect the g factor (vide supra), we decided to prepare molecular analogs as robust, perturbation-free models of the **X** and **S** assemblies, in which two **HH**s are merged at the terminal and central naphthalene moiety to give X-shaped dinaphtho[2,1-*i*:1′,2′-*l*]hexahelicene **DNH** and S-shaped diphenanthro[3,4-*c*:3′,4′-*l*]chrysene **DPC** (Fig. 2a). The structures of such molecules have been theoretically discussed previously[21]. Both **DNH** and **DPC** exhibited extraordinarily intensified CD and CPL responses, as detailed below. State-of-the-art calculations further revealed the decisive role of molecular symmetry (which determines the electric and magnetic transition

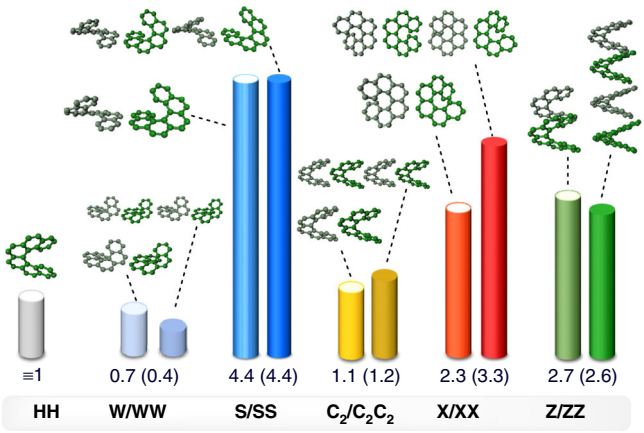

Fig. 1 Design principle for various combinations of chiral monomers. CD intensities (relative g_{abs} against **HH**) predicted by the TD-DFT calculation at the M06-2X/def2-TZVP level for the main band of various **HH** assemblies. Two **HH** units are aligned in figure **W**, **S**, double C ($\mathbf{C_2}$), **X** and **Z** at the vdW contact distance, while the same **W**, **S**, $\mathbf{C_2}$, **X**, or **Z** assembly is repeated horizontally (in **WW**, **SS**, $\mathbf{C_2C_2}$, and **XX**) or vertically (in **ZZ**). The helical axes of **HH**s are sled parallel in **W**, **WW**, $\mathbf{C_2}$, and $\mathbf{C_2C_2}$, or inline parallel in **Z** and **ZZ**, but sled anti-parallel in **S**, **SS**, **X**, and **XX**

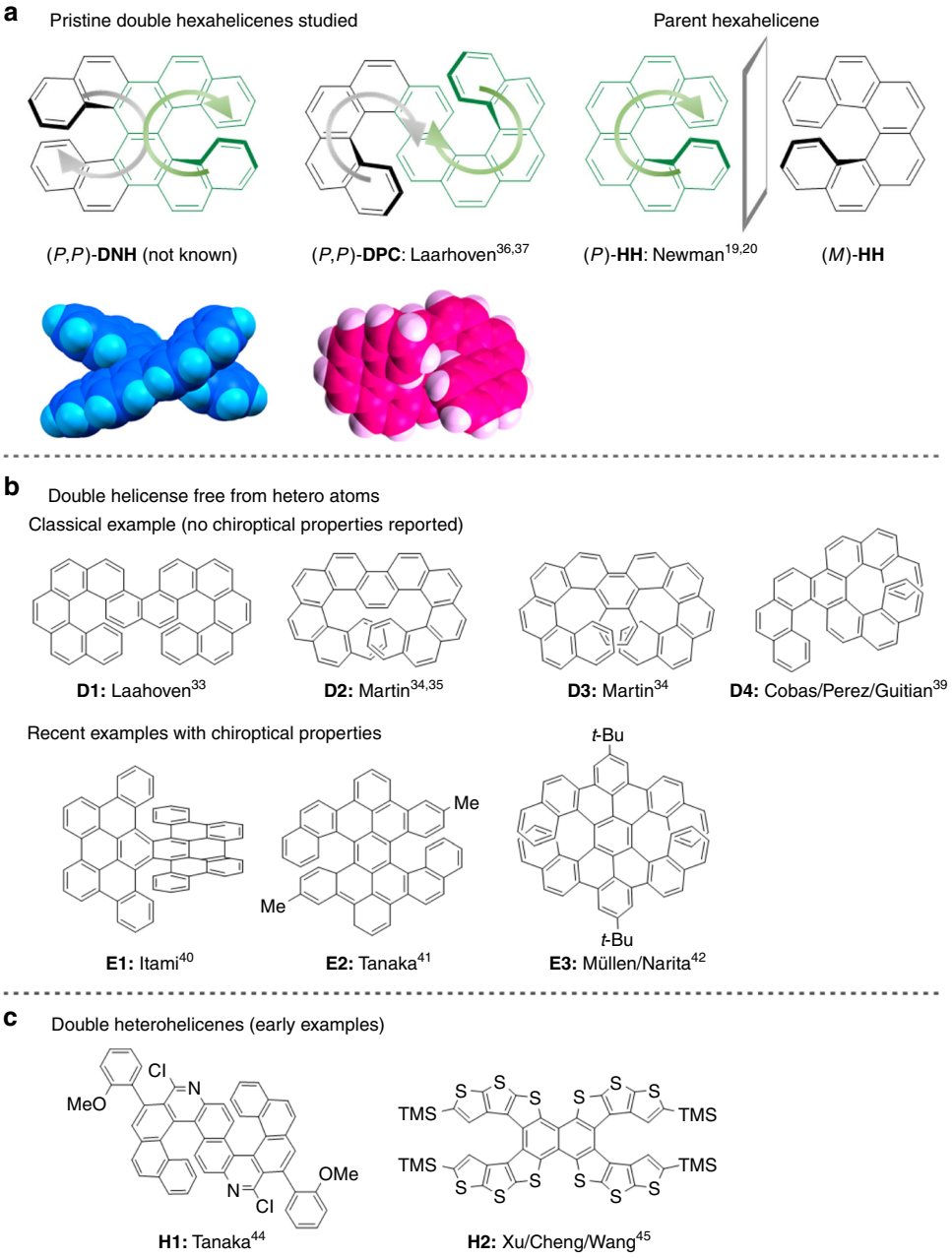

Fig. 2 Double helicenes. **a** Pristine double hexahelicenes (**DNH** and **DPC**, only (*P,P*)-enantiomers are shown for clarity) and the enantiomer pair of parent hexahelicene (**HH**). Structures of **DNH** and **DPC** in racemate crystals are also shown. **b** Selected examples of hetero atom-free double helicenes. **c** Early examples of double heterohelicenes

dipole moments, as well as their relative angle) in attaining the intensified CD and CPL responses of both the double helicenes (Supplementary Table 4). This theory-driven protocol for predicting the ground-state and excited-state chiroptical properties is not restricted to the design of superior chiroptical molecules but is expandable to the design of two-dimensionally and three-dimensionally aligned chiral elements, such as chiral supramolecular assembly[22] and chiral surface organization[23].

Preparation and structure of double hexahelicenes. Double helicenes are an important target of current research[24]. Indeed, somewhat exotic double heterohelicenes, containing boron, nitrogen, sulfur or phosphorous, as well as π-expanded double heterohelicenes, have been reported recently[25–31]. Also, the coordination of (hetero)helicenes with transition metal(s) has been employed for constructing double and higher helicenoids[32]. Nevertheless, unsubstituted double helicenes free from hetero atom are still rare (Fig. 2b, **D1**–**D4**). Beyond the structural perfectness and beauty, pristine double helicenes are indispensable for better scrutinizing how the photophysical, in particular the chiroptical, properties are affected by molecular symmetry in the absence of the electronic and steric perturbations of hetero atom(s) and/or substituent(s). A number of achiral *meso*- and chiral *dl*-double hexahelicenes were reported in the 1970's[33–37]. Some of the latter were optically resolved[38], but chiroptical properties have not been explored yet for these and related[39] double helicenes. Quite recently, the chiroptical properties of three double helicenes with alkyl and/or fused aromatic substituents have become available, but the structure-chiroptical property relationship remain unanswered (Fig. 2b, **E1**–**E3**)[40–42].

Pristine *dl*-double hexahelicenes **DNH** and **DPC**, bearing the C_2-symmetry element along the helical axis, were prepared as racemic mixtures (Fig. 2a). The preparation and diastereomer (*meso*/*dl*) separation of S-shaped **DPC** are known[32,33], but neither crystal structure nor optical resolution has been reported, while X-shaped **DNH** is a new compound. Orange-colored single crystals appropriate for X-ray diffraction analyses were obtained for both the *dl*-double hexahelicenes (Fig. 2a, also see Supplementary Figures 1, 2). The crystal structures of **DNH** and **DPC** were slightly deviated from the theoretically predicted D_2-symmetric and C_2-symmetric structures due to the packing request. Merging two **HH**s brought about further deformation to the resulting double helicenes, which however localized near the central naphthalene unit and hence the original features of **HH** were mostly preserved. In the excited state, the helical pitch was predicted to shrink by 0.2 Å for **HH** but by only 0.1 Å for **DNH** and **DPC**, minimizing the undesired losses of excited-state chiroptical responses of the latter two. Extended discussion on the more detailed structural analyses of **DNH** and **DPC** in the ground and excited states can be found in the Supplementary Discussion, Supplementary Figure 3 and Supplementary Tables 1, 2.

Optical resolution and circular dichroism of double hexahelicenes. **DNH** and **DPC** were optically resolved by chiral HPLC (Supplementary Figures 4, 5). CD spectra of (*P*,*P*)-**DNH** and (*P*,*P*)-**DPC**, as well as (*P*)-**HH**, were recorded in dichloromethane at 25 °C (Fig. 3a); for the corresponding UV–Vis spectra and g_{abs} factor profiles, see Supplementary Figure 6. The absolute configuration was unambiguously assigned by comparing the experimental CD spectrum with the theoretical one calculated by the RI-CC2/def2-TZVPP method (Fig. 3a).

(*P*)-**HH** exhibits positive and negative Cotton effects (CEs) for the ^1B_b and ^1B_a bands, respectively (Fig. 3a). (*P*,*P*)-**DNH** and (*P*,*P*)-**DPC** showed apparently similar positive-negative CEs in the same region, but the molar CD ($\Delta\varepsilon$) for the ^1B_b transition amounted to +650 and +801 $M^{-1}\,cm^{-1}$, respectively, both of which far exceed twice the value for (*P*)-**HH** (+284 $M^{-1}\,cm^{-1}$)[43]. To the best of our knowledge, the $\Delta\varepsilon$ value for **DPC** is the largest ever reported for non-aggregated or non-oligomerized helicenes and helicenoids. Also, the g_{abs} factors for the ^1B_b band of (*P*,*P*)-**DNH** and (*P*,*P*)-**DPC** (+0.016 and +0.022, respectively) are nearly or more than twice the value for (*P*)-**HH** (+0.009), confirming enhanced dissymmetry in the double hexahelicenes.

The *g* factor is an absolute measure of dissymmetry that is already normalized for the transition probability *D* (as $g = 4R/D$), but is not directly correlated with the size of molecule. From the viewpoint of attaining optimal chiroptical responses with minimal resource, the *g* factor per benzene unit (g_{abs}/n) is a more sensible measure of dissymmetry for evaluating and comparing the ability of each benzene unit to induce the overall dissymmetry of helicene. The g_{abs}/n values for the ^1B_b and ^1L_b bands are 1.5×10^{-3} and 2.0×10^{-4} for the parent hexahelicene, respectively, but increase to $1.6–2.2 \times 10^{-3}$ and $2.6–2.8 \times 10^{-4}$ for the double hexahelicenes, respectively. This indicates that the benzene unit in double helicene is 1.1–1.5-fold more efficient than that in single helicene in inducing absorption dissymmetry. This finding that merging two helicenes is 10–50% more resource-efficient than simply assembling them may encourage the molecular, rather than supramolecular, strategy for constructing advanced chiroptical devices.

Electric and magnetic transition dipole moments for ^1B_b transition. In contrast to the effects of helix elongation[39] and substitution[44,45], the effects of symmetry on the chiroptical responses of helicene have been explored only fragmentally. In the pioneering work on S-shaped double azahelicene (**H1**)[46] and X-shaped double thiahelicene (**H2**)[47] (Fig. 2c), the chiroptical properties were described, but no further systematic analyses assisted by theoretical calculations have been done. To better illustrate the origin of the extraordinarily strong chiroptical responses observed for **DNH** and **DPC**, we analyze the experimental CD intensities using the three theoretical parameters, $\boldsymbol{\mu}_e$, $\boldsymbol{\mu}_m$, and θ (Eq. 1), given by the RI-CC2 calculations. As shown in Fig. 3a, our theoretical calculations reproduced the experimental CD spectra quite satisfactorily.

Figure 4 compares the transition dipole moments calculated for the ^1B_b bands of **DNH** and **DPC** with those of **HH**. The ^1B_b transition is characteristic to helicene, being aligned along the helical axis[39]. In X-shaped **DNH**, the ^1B_b band was split into two transitions (Fig. 4 and Supplementary Table 4), the combined $|\boldsymbol{\mu}_e|$

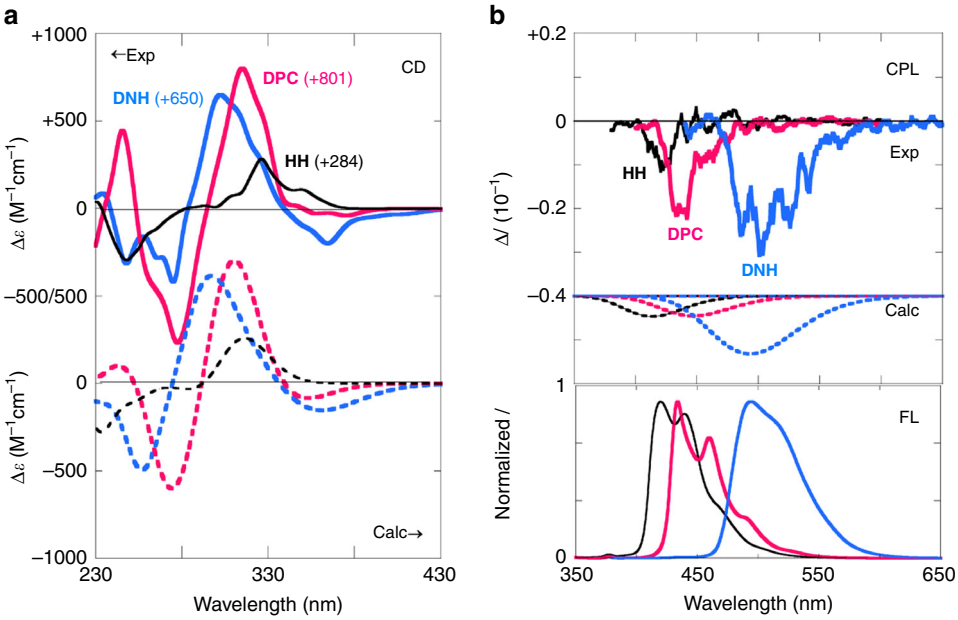

Fig. 3 CD and CPL spectra for double hexahelicenes. **a** Experimental (solid) and theoretical (dashed) CD spectra. **b** Experimental (bold solid) and theoretical CPL (dashed) spectra, as well as experimental fluorescence (solid) spectra. Blue: (*P*,*P*)-**DNH**, red: (*P*,*P*)-**DPC**, black: (*P*)-**HH**

and $|\boldsymbol{\mu}_\mathbf{m}|$ of which were comparable to, or even exceed, those of parent **HH**, while their relative angle θ became nil to maximize the cos θ value to unity in both the transitions that constitute the ^1B_b band of **DNH**. In contrast, the cos θ value for **HH** was mere 0.24 ($\theta = 76°$). In the case of S-shaped **DPC**, $|\boldsymbol{\mu}_\mathbf{e}|$ was reduced by a factor of 0.78, but $|\boldsymbol{\mu}_\mathbf{m}|$ was enhanced by a factor of 1.29, relative to **HH**, to offset each other. This reveals that the parallel alignment ($\theta = 0$) of the two transition moments (Fig. 4) is the major cause of the unprecedentedly large $\Delta\varepsilon$ value of $+801\ M^{-1}\ cm^{-1}$ observed for **DPC**. Intriguingly, the parallel orientation of $\boldsymbol{\mu}_\mathbf{e}$ and $\boldsymbol{\mu}_\mathbf{m}$ in these double helicenes is qualitatively explained as a vector sum of the transition moments of component **HH**s (Fig. 4, dashed arrows). Because of the C_2-symmetry element along the ^1B_b transitions, the vertical components of both transition moments are canceled out and thus the angle θ becomes zero in both the double helicenes.

In brief, the C_2-symmetry element along the helical axis of **DNH** and **DPC** (which is absent in **HH**) parallel-aligns the $\boldsymbol{\mu}_\mathbf{e}$ and $\boldsymbol{\mu}_\mathbf{m}$ moments of the ^1B_b transition to maximize the cos θ value and thus the rotational strength R, eventually achieving the extraordinary CD intensities. Such a symmetry-based strategy to parallel-align the electric and magnetic transition dipole moments for stronger CD have never been proposed but should be more effectively exploited in the design of advanced chiroptical materials.

CPL of double hexahelicenes. The photophysical properties of **DNH** and **DPC** were further examined and compared with those of parent **HH**[48] (Table 1). As shown in Fig. 3b, the fluorescence spectra of **DPC** (and **HH**) have the vibrational fine-structures, while that of **DNH** is more diffused. The fluorescence 0–0 bands of **DNH** and **DPC** appear at 494 and 434 nm, respectively, which are close in energy to the absorption 0–0 bands of the ^1L_b transition observed at 471 and 430 nm (Supplementary Figure 7) to afford the small Stokes shifts of 670 and 210 cm^{-1}, respectively. These observations indicate that the excited-state relaxation from the Franck–Condon state is small in energy (and structure) in these double hexahelicenes. Fluorescence quantum yields (Φ) were 0.018 for **DNH** and 0.041 for **DPC**, which are appreciably smaller or larger than that for **HH** ($\Phi = 0.032$), but much larger than those reported for higher homologs ($\Phi < 0.01$) [49,50], due to the intersystem crossing progressively accelerated with increasing helicene size. The fluorescence lifetimes (τ) followed the same trend; thus, **DPC** gave the longest τ of 10.9 ns and **DNH** the shortest 2.8 ns, while **HH** came in the middle ($\tau = 8.4$ ns). All of these features (i.e., the highly structured, blue-shifted spectra, larger Φ, longer τ and smaller Stokes shift) observed for **DPC**, than for **DNH**, imply that the former is structurally more rigid and deformed than the latter to discourage the conformational and energy relaxation in the excited state.

Despite the strong specific rotation and CD well documented for helicenes, the CPL behavior has attracted less attention until recently[51–53]. The magnitude of CPL is evaluated by the luminescence dissymmetry factor (g_{lum}), which is defined as a relative intensity difference between left-circularly and right-circularly polarized emission. Apart from the exceptionally high g_{lum} factors of $1\text{-}3 \times 10^{-2}$ reported for S-shaped double azahelicenes[42], the g_{lum} factors for single helicenes and helicenoids (free from assembling or aggregation) are in the order 10^{-3}[6,54]. Because the fluorescence of helicene usually occurs from the lowest excited singlet (S_1) state, the g_{lum} factor should correlate with the absorption dissymmetry factor (g_{abs}) for the lowest-energy ^1L_b transition of helicene. Recently, the g_{lum} and g_{abs} factors have been collected for various helicenes to show a good correlation between them: $g_{lum} = 0.61 \times g_{abs}$[6].

Figure 3b, compares the experimental and theoretical CPL spectra and the experimental fluorescence spectra of (*P*,*P*)-**DNH**, (*P*,*P*)-**DPC** and (*P*)-**HH**. All the (*P*)- or (*P*,*P*)-configured single

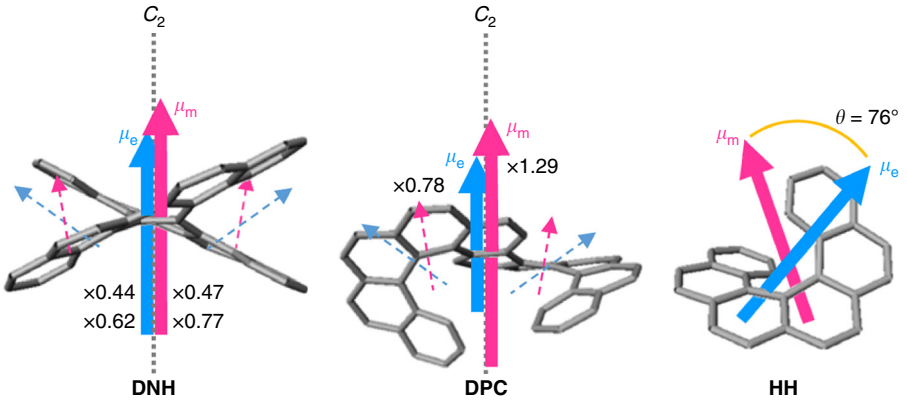

Fig. 4 Transition dipole moments in the ground state. Schematic representations of electric ($\boldsymbol{\mu}_\mathbf{e}$, blue) and magnetic ($\boldsymbol{\mu}_\mathbf{m}$, red) transition dipole moments of the ^1B_b band for X-shaped and S-shaped double hexahelicenes **DNH** and **DPC**, with the magnitudes relative to parent **HH**, calculated at the RI-CC2/def2-TZVPP level. For clarity, the two transitions involved in the ^1B_b band of **DNH** are combined, as their directions are identical. Dashed arrows in double helicenes indicate the transition dipole moments of component **HH**s. See Supplementary Table 4 for further details

Table 1 Photophysical and (Chir)optical properties of (*P*,*P*)-DNH, (*P*,*P*)-DPC and (*P*)-HH

Helicene	λ_{ab}	λ_{fl}	Stokes shift	Φ	τ	λ_p	E_{ST}	$g_{lum}/10^{-3}$	$(g_{lum}/n)/10^{-4}$	$g_{abs}/10^{-3}$	$(g_{abs}/n)/10^{-4}$
DNH	471	494	670	0.018	2.8	672	5390	−2.5	−2.5	−2.6 (+16)	−2.6 (+16)
DPC	430	434	210	0.041	10.9	548	4800	−2.1	−2.1	−2.8 (+22)	−2.8 (+22)
HH	410	420	580	0.032	8.4	526	4780	−0.9	−1.5	−1.2 (+9.2)	−2.0 (+15)

In dichloromethane at 25 °C, unless stated otherwise. λ_{ab}: the 0–0 band of L_b transition in UV–Vis spectrum; λ_{fl}: fluorescence peak maximum (0–0 band); λ_p: phosphorescence peak maximum in ethanol glass at 77 K, all in nm; Stokes shift in cm^{-1}; Φ: fluorescence quantum yield, τ: fluorescence lifetime in ns; E_{ST}: S_1–T_1 energy gap in cm^{-1}; g_{lum}: luminescence dissymmetry factor; g_{abs}: absorption dissymmetry factors for the L_b band and for the ^1B_b band in the parentheses; g/n: dissymmetry factor per benzene unit. See also Supplementary Figures 6, 7

and double hexahelicenes afforded strong negative CPL. In the CPL spectra (Fig. 3b), both the double helicenes exhibited the same-signed CEs for the ^1L_b transition (≥330 nm). Our theoretical calculations at the RI-CC2/def2-TZVPP level well reproduced the sign and emission wavelength of CPL, as well as the relative CPL intensity among the single and double helicenes. Remarkably, the emission of X-shaped **DNH** was greatly red-shifted to 450–600 nm due to the excited-state relaxation facilitated by the effective π-conjugation. (*P*,*P*)-**DNH** and (*P*,*P*)-**DPC** gave the g_{lum} factors of -2.5×10^{-3} and -2.1×10^{-3} (Table 1), which exceeds twice the value for (*P*)-**HH** (-0.9×10^{-3}). The luminescence dissymmetry factor per benzene unit (g_{lum}/n), a quantitative measure of the luminescence dissymmetry caused by each benzene unit, is -1.5×10^{-4} for **HH** but increases up to -2.5×10^{-4}, and -2.1×10^{-4} for **DNH** and **DPC**, respectively, indicating that the double helicenes are 40–70% more resource-efficient in generating CPL, as was the case with CD.

These results demonstrate the advantage of possessing C_2-symmetry element along the helical axis (and the larger excited-state helical pitches) in these double helicenes. Intriguingly, **DNH** exhibits comparable g_{lum} (-2.5×10^{-3}) and g_{abs} (-2.6×10^{-3}), whereas the g_{lum} of **DPC** (-2.1×10^{-3}) is appreciably smaller than the corresponding g_{abs} (-2.8×10^{-3}). Thus, the g_{lum}/g_{abs} ratio as a measure of the excited-state relaxation is close to unity (0.96) for **DNH** but decreases to 0.75 for **DPC**, both of which are larger than or comparable to the value for **HH** (0.75). The g_{lum}/g_{abs} ratios of double helicenes, especially that for **DNH**, are larger than that (0.61) obtained as a global average for all the reported helicenes[6], confirming the increased rigidity of **DNH**. The structured fluorescence and CPL spectra urge us to take the vibrational effects into consideration for a more rigorous comparison of the CPL data, which is however not immediately feasible at the level of theory employed and will not be discussed further here. Recently, the importance of vibrational coupling in analyzing the structured CD and CPL spectra of some hexahelicenes has been critically assessed by applying the harmonic approximation to the theoretical treatment[55,56].

Electric and magnetic transition dipole moments of ^1L_b transition. Figure 5 illustrates the dipole moments of the ^1L_b transition of **DNH**, **DPC**, and **HH** calculated for the excited state. The corresponding moments in the ground state are shown in Supplementary Figure 8. These two sets of calculations enable a simulation of the CD and CPL responses upon upward S_0-to-S_1 and downward S_1-to-S_0 transition, respectively. As discussed above, the rotational strengths (*R*) of absorption and emission are functions of the relevant $\boldsymbol{\mu}_e$, $\boldsymbol{\mu}_m$, and θ. The small *R* of −0.5 for the ^1L_b band of **HH** can be traced back to the nearly orthogonal electric and magnetic dipole moments for the upward transition: $\theta = 94°$ (or 96°)[39,47]. The angle θ for the downward transition (CPL) was found appreciably increased to 112°. This apparently small change in θ alone would enhance the *R*-value by a factor of 5 (as cos 112°/cos 94° = 0.37/0.07) but is nearly canceled out by the smaller $|\boldsymbol{\mu}_m|$ value arising from the decrease in helical pitch to eventually give a comparable *R*-value of −0.6 for CPL. The increased $|\boldsymbol{\mu}_e|$ values for the double helicenes in the ground and excited states are attributable to the extended π-conjugation, as **DNH** and **DPC** contain two **HH** units merged in a single molecule.

In S-shaped **DPC**, the angle θ in the ground state was calculated as 95°, almost identical to that of **HH**. Therefore, the more than doubled g_{abs} factor for the ^1L_b band (from -1.2×10^{-3} for **HH** to -2.8×10^{-3}) should be attributed not to θ but to $|\boldsymbol{\mu}_e|$ and $|\boldsymbol{\mu}_m|$ increased by the extended π-conjugation. For the downward transition, θ was further increased to 130°, meaning 7.4-fold enhancement in *R* (cos 130°/cos 95° = 0.64/0.09) by this factor alone. Indeed, the CPL observed for **DPC** became considerably stronger (by a factor of 2.3) than that of **HH**.

In X-shaped **DNH**, the π-conjugation is extended to supplement the C_2-symmetric nature of the parent helicene unit and hence the orientation of ^1L_b transition becomes nearly orthogonal to that of **HH** or **DPC**, being aligned along the helical axis. Hence, the $\boldsymbol{\mu}_e$ and $\boldsymbol{\mu}_m$ moments are aligned antiparallel, optimizing the orientation factor (cos 180° = −1) in *R*. However, because of the additional C_2-symmetry element in D_2 symmetry across the direction of angular momentum, the $|\boldsymbol{\mu}_m|$ was substantially reduced to only moderately enhance the CPL. Nevertheless, the contribution of θ outweighs that of $\boldsymbol{\mu}_m$ to afford the g_{lum} of -2.5×10^{-3}, which is 2.8-fold larger than that of **HH**. The contributions of $\boldsymbol{\mu}_e$ and $\boldsymbol{\mu}_m$ are larger in the excited state than in the ground state for both **DNH** and **DPC**, reflecting their less contracted helical pitches relative to **HH**.

Discussion

In this proof-of-concept study employing X-shaped and S-shaped prsistine double hexahelicenes (**DNH** and **DPC**) as representative molecular models, we have developed a theory-guided, symmetry-based protocol for designing advanced molecular and supramolecular chiral systems with enhanced ground-state and excited-state chiroptical responses (CD and CPL), where the alignment of chiral elements plays a decisive role. Thus, **DNH** and **DPC**, constructed by merging two hexahelicenes (**HH**) in D_2 and C_2 symmetry, achieved the absorption dissymmetry factors per benzene unit (g_{abs}/n) for the ^1B_b band that are larger by a factor of up to 1.5 than that of parent **HH**. This enhancement was well rationalized by the electric ($\boldsymbol{\mu}_e$) and magnetic ($\boldsymbol{\mu}_m$) transition dipole moments and their

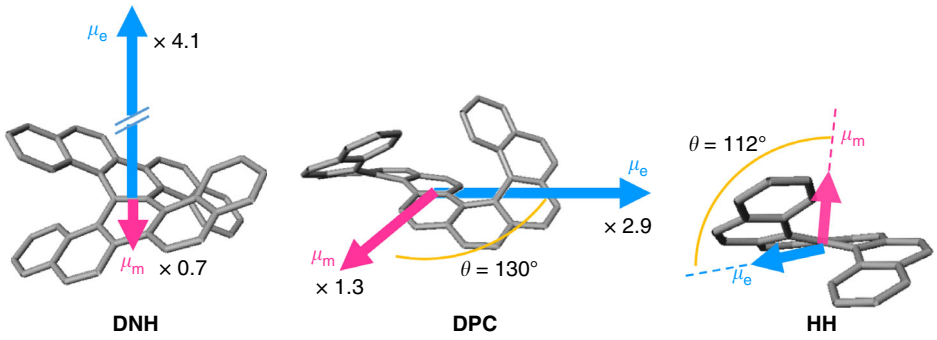

Fig. 5 Transition dipole moments in the excited state. Schematic representations of the electric ($\boldsymbol{\mu}_e$, blue) and magnetic ($\boldsymbol{\mu}_m$, red) transition dipole moments of the ^1L_b band of **DNH** and **DPC** in the excited states, with the magnitudes relative to those for parent **HH**, calculated at the RI-CC2/def2-TZVPP level. The corresponding moments in the ground state are shown in Supplementary Figure 8. Also see Supplementary Table 4 for further details

relative angle (θ) evaluated theoretically. In the double helicenes, $\boldsymbol{\mu}_e$ and $\boldsymbol{\mu}_m$ were parallel-aligned ($\theta = 0$) to maximize the orientation factor (cos θ) up to unity, which was mere 0.24 (cos 76°) in **HH**, while $|\boldsymbol{\mu}_e|$ and $|\boldsymbol{\mu}_m|$ were comparable or only slightly improved. Also, the luminescence dissymmetry factor per benzene unit (g_{lum}/n) was up to 1.7-fold larger for the double helicenes than for **HH**, for which the increased $|\boldsymbol{\mu}_e|$ and θ are responsible. The enhanced g_{abs}/n and g_{lum}/n values for double helicenes mean that merging two helicenes is 50–70% more resource-efficient than simply assembling them, which may encourage the molecular, rather than supramolecular, strategy for constructing advanced chiroptical devices.

Our combined experimental and theoretical investigations have further revealed how the molecular symmetry and the alignment of chiral elements determine the CD and CPL responses by manipulating $\boldsymbol{\mu}_e$, $\boldsymbol{\mu}_m$ and θ. The theoretical analyses deliver an intriguing implication that non-covalently aligning multiple chiral units into a chiral supramolecular assembly is less resource-efficient than merging the same units in a single molecule. Nevertheless, the chiroptical responses of supramolecular assembly are not very sensitive to the inter-chromophore distance to allow compartmentalized assembling of chiral elements in supramolecular/macromolecular/crystal lattices and channels without deteriorating the enhanced chiroptical properties. These results and concepts as well as the insights derived therefrom provide a reliable guiding principle for designing novel advanced chiral molecules and materials with strong chiroptical responses. The basic concepts should be expandable to nano-chirality and mesoscopic chirality composed of numerous rationally organized chiral elements.

Methods

Preparation of double hexahelicenes. Full details of general methods, synthetic procedures, and characterization data can be found in the Supplementary Methods. The preparation of racemic double hexahelicene **DPC** was already described[33]. Another double hexahelicene **DNH** was prepared from 7,10-dimethylhexahelicene. This helicene was brominated with *N*-bromosuccinimide to 7,10-bis(bromomethyl)hexahelicene, which was transformed to the corresponding phosphonium salt. The reaction of this salt with *o*-iodobenzoaldehyde afforded an isomeric mixture of 7,10-bis[2-(2-iodophenyl) ethenyl]hexahelicenes. Through silica-gel column chromatography, the desired (*Z,Z*)-isomer, suitable for photocyclization, was isolated. The photocyclization was performed at wavelengths >280 nm in the presence of iodine and tetrahydrofuran in a flow reactor equipped with a high-pressure mercury lamp to afford the desired **DNH** as a crude racemic mixture. The optical resolutions of **DNH** and **DPC** were performed by chiral HPCL using Daicel Chiralpak IA and IB column, respectively, eluted with hexane-dichloromethane with or without ethanol. Crystals suitable for X-ray diffraction analysis were obtained by slow evaporation of solutions of racemic **DNH** or **DPC** and the cif files of these and related molecules can be found in Supplementary Data 1. ^{1}H and ^{13}C NMR spectra of all compounds are presented in Supplementary Figures 10–27.

Computational details. Theoretical calculations were performed on Linux PCs by using the Turbomole or the Gaussian program suite. The TD-DFT calculations on model systems were performed at the M06-2X/def2-TZVP level. Ground-state geometries were fully optimized at the dispersion-corrected density functional theory (3rd generation, DFT-D3 with BJ dumping), using the AO basis-set of valence triple-ξ quality (def2-TZVPP) with the resolution of identity (RI) approximation. Excited-state structures were optimized by the time-dependent, second-order approximate coupled-cluster singles and doubles model, in conjunction with the resolution-of-identity method (RI-CC2 method) with the def2-TZVPP basis-set. The UV–Vis, CD, and CPL spectra were calculated by the same level of theory and the rotational strengths obtained in length gauge were expanded by Gaussian functions, where the bandwidth at 1/*e* height is fixed at 0.5 eV, unless otherwise stated. Further experimental details can be found in the Supplementary Methods, and the optimized geometries in Supplementary Table 5. Calculated molecular orbitals for **DNH**, **DPC**, and **HH** can be found in Supplementary Figure 9.

Data availability. The X-ray crystallographic coordinates for structures reported in this Article have been deposited at the Cambridge Crystallographic Data Center (CCDC), under deposition number CCDC 1826743-1826746. These data can be obtained free of charge from The CCDC via www.ccdc.cam.ac.uk/data_request/cif. The additional data that support the findings of this study are available from the corresponding author upon reasonable request.

Received: 2 May 2018 Accepted: 31 May 2018
Published online: 05 July 2018

References

1. Brandt, J. R., Salerno, F. & Fuchter, M. J. The added value of small-molecule chirality in technological applications. *Nat. Rev. Chem.* **1**, 0045 (2017).
2. Rickhaus, M., Mayor, M. & Juricek, M. Strain-induced helical chirality in polyaromatic systems. *Chem. Soc. Rev.* **45**, 1542–1556 (2016).
3. Rosenfeld, L. Quantenmechanische Theorie der Natürlichen optischen aktivität von Flüssigkeiten und Gasen. *Z. Phys.* **52**, 161–174 (1929).
4. Schellman, J. A. Circular dichroism and optical rotation. *Chem. Rev.* **75**, 323–331 (1975).
5. Warnke, I. & Furche, F. Circular dichroism: electronic. *Wiley Interdiscip. Rev.: Comput. Mol. Sci.* **2**, 150–166 (2012).
6. Tanaka, H., Inoue, Y. & Mori, T. Circularly polarized luminescence and circular dichroism in small organic molecules: correlation between excitation and emission dissymmetry factors. *ChemPhotoChem* **2**, 386–402 (2018).
7. Sato, S. et al. Chiral intertwined spirals and magnetic transition dipole moments dictated by cylinder helicity. *Proc. Nat. Acad. Sci. USA* **114**, 13097–13101 (2017).
8. Nakakuki, Y., Hirose, T., Sotome, H., Miyasaka, H. & Matsuda, K. Hexa-*peri*-hexabenzo[7]helicene: Homogeneously π-extended helicene as a primary substructure of helically twisted chiral graphenes. *J. Am. Chem. Soc.* **140**, 4317–4326 (2018).
9. Dhbaibi, K. et al. Exciton coupling in diketopyrrolopyrrole-helicene derivatives leads to red and near-infrared circularly polarized luminescence. *Chem. Sci.* **9**, 735–742 (2018).
10. Shen, Y. & Chen, C.-F. Helicenes: Synthesis and applications. *Chem. Rev.* **112**, 1463–1535 (2012).
11. Gingras, M. One hundred years of helicene chemistry. *Part 3: Appl. Prop. carbohelicenes. Chem. Soc. Rev.* **42**, 1051–1095 (2013).
12. Meurer, K. P. & Vögtle, F. Helical molecules in organic chemistry. *Top. Curr. Chem.* **127**, 1–76 (1985).
13. Martin, R. H. The helicenes. *Angew. Chem. Int. Ed.* **13**, 649–660 (1974).
14. Hasan, M. & Borovkov, V. Helicene-based chiral auxiliaries and chirogenesis. *Symmetry* **10**, 10 (2018).
15. Ernst, K.-H. Stereochemical recognition of helicenes on metal surfaces. *Acc. Chem. Res.* **49**, 1182–1190 (2016).
16. Isla, H. & Crassous, J. Helicene-based chiroptical switches. *C. R. Chim.* **19**, 39–49 (2016).
17. Bosson, J., Gouin, J. & Lacour, J. Cationic triangulenes and helicenes: synthesis, chemical stability, optical properties and extended applications of these unusual dyes. *Chem. Soc. Rev.* **43**, 2824–2840 (2014).
18. Yang, Y., da Costa, R. C., Fuchter, M. J. & Campbell, A. J. Circularly polarized light detection by a chiral organic semiconductor transistor. *Nat. Photon.* **7**, 634–638 (2013).
19. Newman, M. S., Lutz, W. B. & Lednicer, D. A new reagent for resolution by complex formation; the resolution of phenanthro-[3,4-*c*]phenanthrene. *J. Am. Chem. Soc.* **77**, 3420–3421 (1955).
20. Newman, M. S. & Lednicer, D. The synthesis and resolution of hexahelicene. *J. Am. Chem. Soc.* **78**, 4765–4770 (1956).
21. Bachrach, S. M. Double helicenes. *Chem. Phys. Lett.* **666**, 13–18 (2016).
22. Valera, J. S., Gómez, R. & Sánchez, L. Supramolecular polymerization of [5] helicenes. Consequences of self-assembly on configurational stability. *Org. Lett.* **20**, 2020–2023 (2018).
23. Stetsovych, O. et al. From helical to planar chirality by on-surface chemistry. *Nat. Chem.* **9**, 213–218 (2016).
24. Li, C., Yang, Y. & Miao, Q. Recent progress in chemistry of multiple helicenes. *Chem. Asian J.* **13**, 884–894 (2018).
25. Wang, X.-Y. et al. Synthesis, structure, and chiroptical properties of a double [7]heterohelicene. *J. Am. Chem. Soc.* **138**, 12783–12786 (2016).
26. Katayama, T. et al. Two-step synthesis of boron-fused double helicenes. *J. Am. Chem. Soc.* **138**, 5210–5213 (2016).
27. Sakamaki, D., Kumano, D., Yashima, E. & Seki, S. A facile and versatile approach to double *N*-heterohelicenes: tandem oxidative C-N couplings of *N*-heteroacenes via cruciform dimers. *Angew. Chem. Int. Ed.* **54**, 5404–5407 (2015).
28. Chen, F. et al. Closed pentaaza[9]helicene and hexathia[9]/[5]helicene: oxidative fusion reactions of *ortho*-phenylene-bridged cyclic hexapyrroles and hexathiophenes. *Angew. Chem. Int. Ed.* **56**, 14688–14693 (2017).
29. Hashimoto, S., Nakatsuka, S., Nakamura, M. & Hatakeyama, T. Construction of a highly distorted benzene ring in a double helicene. *Angew. Chem. Int. Ed.* **53**, 14074–14076 (2014).
30. Ferreira, M. et al. A naphtho-fused double [7]helicene from a maleate-bridged chrysene trimer. *Angew. Chem. Int. Ed.* **56**, 3379–3382 (2017).

31. Satoh, M., Shibata, Y. & Tanaka, K. Enantioselective synthesis of fully benzenoid single and double carbohelicenes via gold-catalyzed intramolecular hydroarylation. *Chem. Eur. J.* **24**, 5434–5438 (2018).
32. Saleh, N., Shen, C. & Crassous, J. Helicene-based transition metal complexes: synthesis, properties and applications. *Chem. Sci.* **5**, 3680–3694 (2014).
33. Laarhoven, W. H. & De Jong, M. H. Photodehydrocyclizations of stilbene-like compounds. VIII. Synthesis of hexaheliceno[3,4-C.]hexahelicene. *Recl. Trav. Chim. Pays-Bas* **92**, 651–657 (1973).
34. Martin, R. H., Eyndels, C. & Defay, N. Double helicenes. Diphenanthro[4,3-*a*;3',4'-*o*]picene and benzo[*s*]diphenanthro[4,3-*a*;3',4'-*o*]picene. *Tetrahedron* **30**, 3339–3342 (1974).
35. Marsh, W. & Dunitz, J. D. Crystal structure of a double helicene, diphenanthro[4,3-*a*; 3',4'-*o*]picene. *Bull. Soc. Chim. Belg.* **88**, 847–852 (1979).
36. Laarhoven, W. H. & Cuppen, T. J. H. M. Photodehydrocyclizations of stilbene-like compounds. IV. Synthesis of a double helicene. rac. and meso diphenanthro [3,4-*c*:3'4'-*l*]chrysene. *Tetrahedron Lett.* **12**, 163–164 (1971).
37. Laarhoven, W. H. & Cuppen, T. H. J. M. Photodehydrocyclizations of stilbene-like compounds VII: synthesis and properties of the double helicene, diphenanthro[3,4-*c*;3',4'-*l*]chrysene. *Recl. Trav. Chim. Pays-Bas* **92**, 553–562 (1973).
38. Mikes, F., Boshart, G. & Gil-Av, E. Resolution of optical isomers by high-performance liquid chromatography, using coated and bonded chiral charge-transfer complexing agents as stationary phases. *J. Chromatogr.* **122**, 205–221 (1976).
39. Pena, D., Cobas, A., Perez, D., Guitian, E. & Castedo, L. Dibenzo[*a,o*] phenanthro[3,4-*s*]pycene, a configurationally stable double helicene: synthesis and determination of its conformation by NMR and GIAO calculations. *Org. Lett.* **5**, 1863–1866 (2003).
40. Fujikawa, T., Segawa, Y. & Itami, K. Synthesis, structures, and properties of π-extended double helicene: a combination of planar and nonplanar π-systems. *J. Am. Chem. Soc.* **137**, 7763–7768 (2015).
41. Yamano, R., Shibata, Y. & Tanaka, K. Synthesis of single and double dibenzohelicenes via rhodium-catalyzed intramolecular [2+2+2] and [2+1 +2+1] cycloadditions. *Chem. Eur. J.* **24**, 6364–6370 (2018).
42. Hu, Y. et al. Benzo-fused double [7]carbohelicene: synthesis, structures, and physicochemical properties. *Angew. Chem. Int. Ed.* **56**, 3374–3378 (2017).
43. Nakai, Y., Mori, T. & Inoue, Y. Theoretical and experimental studies on circular dichroism of carbo[*n*]helicenes. *J. Phys. Chem. A* **116**, 7372–7385 (2012).
44. Nakai, Y., Mori, T. & Inoue, Y. Circular dichroism of (di)methyl- and diaza[6] helicenes. A combined theoretical and experimental study. *J. Phys. Chem. A* **117**, 83–93 (2013).
45. Nakai, Y., Mori, T., Sato, K. & Inoue, Y. Theoretical and experimental studies of circular dichroism of mono- and diazonia[6]helicenes. *J. Phys. Chem. A* **117**, 5082–5092 (2013).
46. Nakamura, K., Furumi, S., Takeuchi, M., Shibuya, T. & Tanaka, K. Enantioselective synthesis and enhanced circularly polarized luminescence of S-shaped double azahelicenes. *J. Am. Chem. Soc.* **136**, 5555–5558 (2014).
47. Liu, X. et al. Synthesis for the mesomer and racemate of thiophene-based double helicene under irradiation. *J. Org. Chem.* **78**, 6316–6321 (2013).
48. Donckt, E. V., Nasielski, J., Greenleaf, J. R. & Birks, J. B. Fluorescence of the helicenes. *Chem. Phys. Lett.* **2**, 409–410 (1968).
49. Sapir, M. & Donckt, E. V. Intersystem crossing in the helicenes. *Chem. Phys. Lett.* **36**, 108–110 (1975).
50. Birks, J. B., Birch, D. J. S., Cordemans, E. & Vander Donckt, E. Fluorescence of the higher helicenes. *Chem. Phys. Lett.* **43**, 33–36 (1976).
51. Abbate, S. et al. Helical sense-responsive and substituent-sensitive features in vibrational and electronic circular dichroism, in circularly polarized luminescence, and in Raman spectra of some simple optically active hexahelicenes. *J. Phys. Chem. C.* **118**, 1682–1695 (2014).
52. Otani, T. et al. Facile two-step synthesis of 1,10-phenanthroline-derived polyaza[7]helicenes with high fluorescence and CPL efficiency. *Angew. Chem. Int. Ed.* **56**, 3906–3910 (2017).
53. Sakai, H. et al. Highly fluorescent [7]carbohelicene fused by asymmetric 1,2-dialkyl-substituted quinoxaline for circularly polarized luminescence and electroluminescence. *J. Phys. Chem. C.* **119**, 13937–13947 (2015).
54. Sánchez-Carnerero, E. M. et al. Circularly polarized luminescence from simple organic molecules. *Chem. Eur. J.* **21**, 13488–13500 (2015).
55. Liu, Y. et al. Vibronic coupling explains the different shape of electronic circular dichroism and of circularly polarized luminescence spectra of hexahelicenes. *J. Chem. Theory Comput.* **12**, 2799–2819 (2016).
56. Weigang, O. E. Emission polarization and circular dichroism of hexahelicene. *J. Chem. Phys.* **45**, 1126–1134 (1966).

Acknowledgements

Financial supports by Grant-in-Aids for Scientific Research, Challenging Exploratory Research, Promotion of Joint International Research (Fostering Joint International Research), and on Innovative Areas "Photosynergetics" (Grant Numbers JP15H03779, JP15K13642, JP16KK0111, JP17H05261, JP18H01964) from JSPS and by the Asahi Glass Foundation are gratefully acknowledged.

Author contributions

M.I. performed preliminary experiments on double hexahelicenes. H.T. prepared double hexahelicenes and performed spectral investigations and analysed the data. H.T. and Y.K. performed the CPL experiments. T.M. planned the project, supervised, performed the quantum chemical calculations, analysed the results, and wrote the paper. M.F. and Y.I. contributed to writing the paper. All the authors discussed the results and commented on the manuscript.

Additional information

Supplementary information accompanies this paper at https://doi.org/10.1038/s42004-018-0035-x.

Competing interests: The authors declare no competing interests.

Reprints and permission information is available online at http://npg.nature.com/reprintsandpermissions/

Publisher's note: Springer Nature remains neutral with regard to jurisdictional claims in published maps and institutional affiliations.